

Experimental evaluation of the stall characteristics of a two-element high-lift airfoil

David Hahn*, Peter Scholz† and Rolf Radespiel‡

*Institute of Fluid Mechanics, Technische Universität Braunschweig,
38106 Braunschweig, Germany*

Abstract

The present contribution describes measurements on a two-element airfoil in a small sized wind tunnel with emphasis on the determination of the stall behaviour. Pressure measurement and oil flow visualisation are the main detection methods used in this work. The influence of side wall boundary layers (BLs) towards stall behaviour and local leading edge droop as compensation, is discussed. The devices realising local droop, the side wall droop-nose (SWDN), were investigated towards droop angles and shape sensitivities. The experimental set-up was examined regarding structural integrity and influences towards the free flow. As a summary, a comparison to other experimental set-ups is given. The best SWDN angle for the investigated configuration was found at 15° and an optimisation of the geometry advantageous to CFD was found. Due to structural stability support devices were introduced, and their impact towards the free flow was characterised. With the investigated adaptations, the size of the wind tunnel has been turned into a minor criteria within the following investigations.

1 Introduction

The prediction of flow separations and hence maximum lift and airfoil stall is still a challenging task for state-of-the-art numerical codes. The major challenges are the three-dimensionality, the unsteadiness, and the diffusive, non-isotropic and non-homogeneous character of separated flows. Therefore, in order to validate numerical codes for such flows, a comprehensive database of the underlying flow phenomena must be gathered. The DFG FOR 1066 has taken the challenge to empower the CFD code TAU to simulate the stall behaviour of an airfoil under disturbed conditions. The disturbances of interest simulate those in atmospherical surrounding. As airplanes operate in the turbulent BL of the atmosphere during the landing approach or the take off phase, the stall behavior of a high-lift airfoil configuration is of great importance. As

*Research Engineer.

†Head of Group “Flow Control and Measuring Techniques”.

‡Professor and Head of Institute.

multi-element airfoils are state of the art airplane wing configurations, a two-element (“slat less”) airfoil, based on the DLR-F 15 airfoil contour, has been chosen as reference airfoil. It is known from other experiments, that this airfoil exhibits a complicated system of separations (flap trailing-edge, flap cove, slat cove, main-element trailing-edge, etc.), which leads to final airfoil stall [14, 16]. Therefore, this airfoil represents a very interesting case for investigations. The stall of single-element airfoils in steady conditions is relatively well documented [5, 17]. High-quality measurements on multi-element airfoils with special emphasis on separations have been performed [1, 15], but failed to cover the stall regime sufficiently detailed. In the field of active flow control, some measurements of a multi-element airfoil in stall condition were realised [14, 16], but considered steady inflow condition only. The establishment of a consistent validation data base looking at a multi element airfoil in steady and disturbed flow is not available but becomes necessary for validating the numerical code.

The DLR-F 15 is a modular construction that was built for industrial (commercial) wind tunnels. Although the large size of industrial tunnels is advantageous towards reduction of wind tunnel influences, large tunnels are barely suitable for the generation of a comprehensive database, as measurement time is severely restricted. This is the reason why the present contribution makes use of a smaller wind tunnel in contradiction to the size advantages, which gain even more importance for airfoils with separated airflow. As the DLR-F 15 in high lift configuration is an airfoil with separated airflow at high angles of attack, the experimental set-up in itself must be analysed and validated with respect to wind tunnel influences. The separated airflow is also responsible for the high level of caution that must be taken during the experiments. During the current investigations, one of the major tasks was to establish a 2-D flow behaviour over the airfoil’s centre section. The aim was the comparability of measurements with 2-D numerical calculations. The determination and minimisation of wind tunnel side wall boundary layers’ (BLs) influence on the airfoil stall was therefore of utmost importance. As the side wall BLs thicken right from the end of the tunnel nozzle, they become more sensitive to additional disturbances. At the intersection between the airfoil and the wind tunnel, the side wall BL, as well as the airfoil BL, are subject to severe adverse pressure gradients. Whereas the airfoil BL is relatively thin and undisturbed, the side wall BL is already thick, which is why profiles tend to stall first near the side walls.

Traditionally active flow control, vortex generators, strakes, local modification of the pressure distribution, or full 3-D design of the airfoil or side walls have been means applied to reduce the effect of side wall BLs interactions with the airfoil flow. However, every method has its pros and cons towards experimental or computational aspect. Active flow control (e.g. suction or blowing) is strongly dependent on the suction / blowing amplitude, pulse rate, position, etc., and is therefore not necessarily objective [12, 7, 8, 9, 13]. In terms of CFD simulation, it might involve a large computational effort. Vortex generators or strakes on their side are proved and objective devices [7, 2]. However, they have a limited range of effectiveness and they require a very large computational effort in CFD simulations. To locally modify the pressure distribution of the airfoil by changing $c_{n,p}$ is apparently an objective, variable, reproducible and robust mean [6]. The comparative effort in CFD computations seems to be relatively moderate. A full 3-D design of the airfoil or side walls towards 2-D behaviour in the centre section is a great design effort and once implemented not variable during tests [3, 10]. Within the current project the establishment of a consistent validation data bases asked for a high reproducibility of the tests. As measurements have to be gathered through multiple campaigns, an easy to install and operate mean is preferable. A disturbed flow and a reasonable effort in CFD simulation advice an as simple as possible set-up. Therefore, the side wall droop-nose (SWDN) was cho-

sen as a device to locally modified the pressure distribution on the airfoil, as it was an elegant compromise between those two aforementioned requirements.

2 Experimental set-up

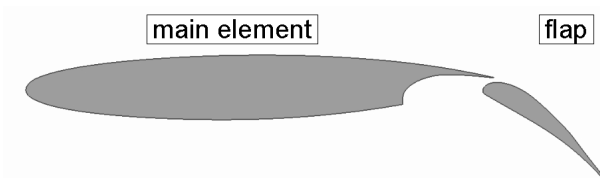


Figure 1: Sketch of the airfoil configuration

The airfoil used for this investigation (Figure 1), was built out of carbon fibre-reinforced plastics (CRP). The contour duplicated the so-called DLR-F 15 in 2e-configuration, consisting of a 89% main-element and a slotted 23% trailing-edge flap. The model was scaled to 0.6 m reference chord length. The airfoil was mounted horizontally in the test-section and was

equipped with two 130 mm (10 % of the wingspan) SWDNs (Figure 2). The angle of attack of a fixed wing-flap configuration can be varied by the use of an α -device. The α -device is an electro motor driven device that introduces the torque equally on both sides into the airfoil configuration. On the other hand, the configuration of the trailing-edge flap can be changed by the use of different acrylic glass inlays, on which the flap is mounted (Figure 2). The investigated flap configuration (called fs#1 in accordance with [14]) has a flap angle of

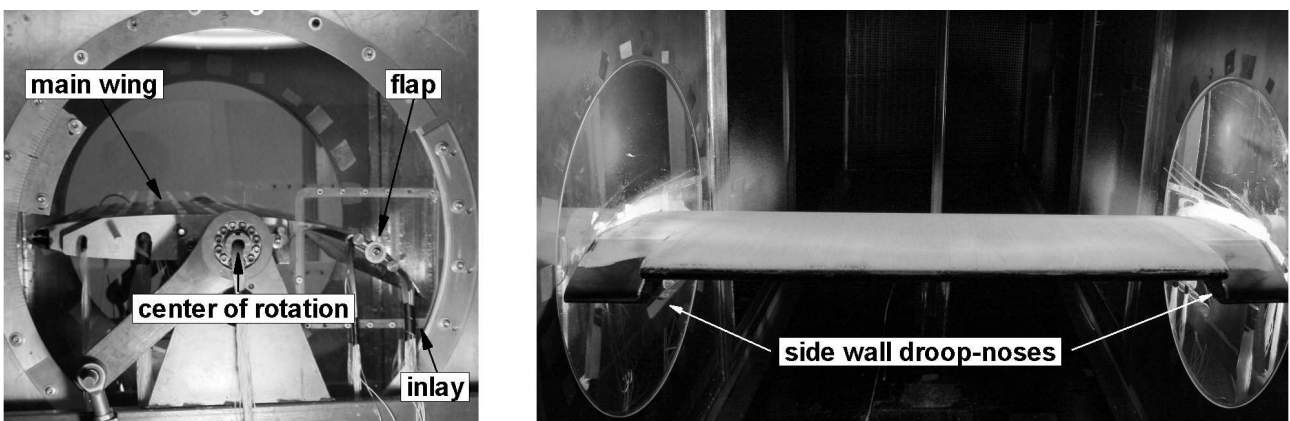


Figure 2: DLR-F 15 airfoil integrated in the MUB test-section

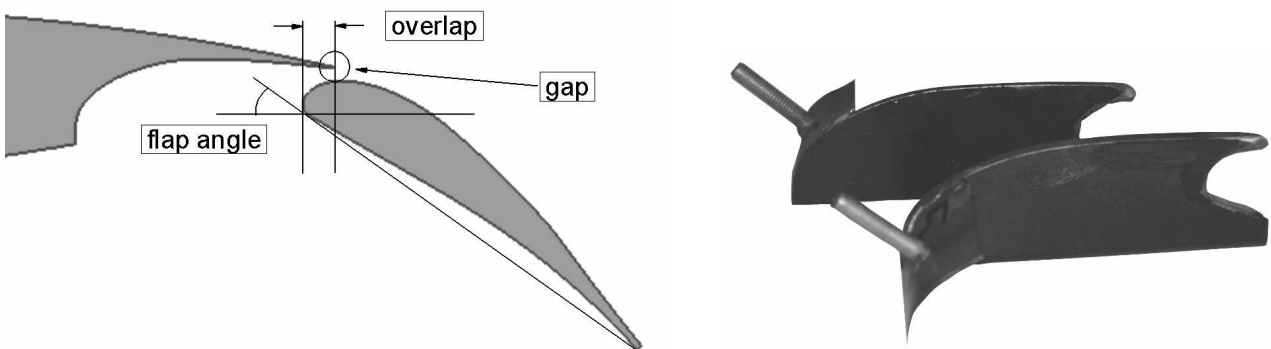


Figure 3: Definition of various measures and illustration of flap-tracks

35°, a gap of 0.8% g_F/c , and an overlap of 2.3% ovl_F/c (Figure 3). Optionally, flap-tracks can be mounted at 1/3 of the wingspan to enhance the stability of the gap and the overlap during all phases of measurement. The flap-tracks were designed as additional support and are expected to incur minimal interference to the flow. The main-element was equipped with 55 pressure measurement taps along the wing centre section, and with 20 taps along each of the two outer sections (Figure 4). With the aid of a PSI 8400 SDI multichannel pressure scanner

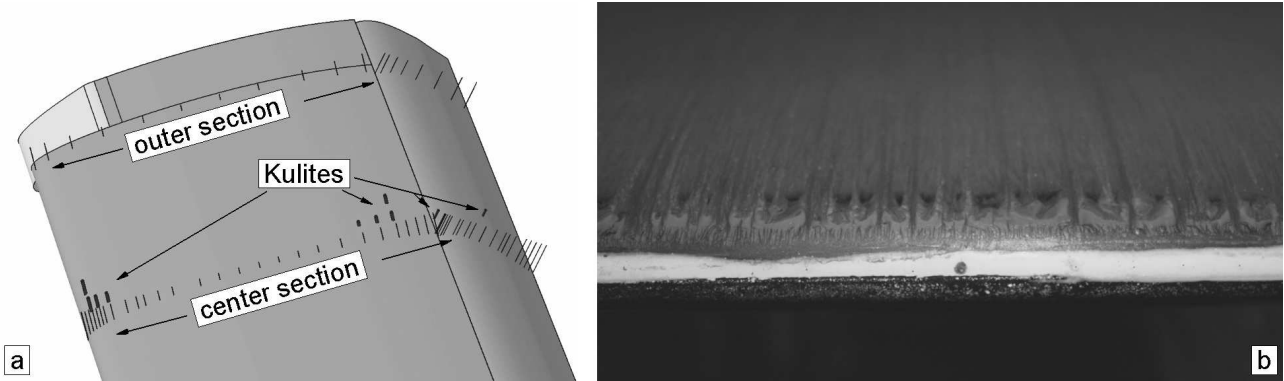


Figure 4: Pressure measurement tap distribution: cord wise a, leading edge wise b

(0.05 % full scale output accuracy), these holes were used for static pressure measurements. In addition, 120 tap holes were integrated into the leading edge of the main-element at 1 % of the reference cord length. They can be used either for measuring the spanwise pressure distribution or for pneumatic tripping that fixes the transition location. Additionally, 8 time resolved pressure transducers (Kulite XCQ 93) were integrated along the centre section of the main-element. Four of the Kulites were placed close to the leading-edge and four close to the trailing-edge so that a span wise alternating pressure distribution could be detected (Figure 4). The flap was equipped with 30 taps along the centre section, and 10 taps along each of the outer section. Additional two time resolved pressure measurement devices were integrated into the flap (Figure 4).

For the determination of the airfoil's drag a wake rake measuring the static pressure distribution over the wake was installed approximately one cord length behind the airfoil. Due to limited number of channels on the PSI system, simultaneous measurement of the pressure distribution over the airfoil and the wake was not possible. Therefore, measurements were performed separately. However the current configuration created strong vortices, that made the wake measurements without interference effects from the wind tunnel walls or the wake-rake itself difficult. Initial results show, that $c_{n,p}$ is in good agreement with c_l , thus making the drag irrelevant. This conclusion rendered the static pressure distribution over the airfoil ($c_{n,p}$) a measure very similar to lift (c_l). As described in the introduction, a non-commercial wind tunnel offers the opportunity of more comprehensive measurement campaigns. Therefore the MUB (Modell-Unterschallwindkanal Braunschweig), a closed-return wind tunnel with a $1.3 \times 1.3 \times 6 \text{ m}^3$ closed, atmospheric test-section was chosen (Figure 5). The wind tunnel is powered by a 300 kW direct current motor, and has a turbulence level of $Tu = 0.20 \%$ at 53 m/s. A heat exchanger in the settling chamber allows constant flow temperature at approximately 10 K above ambient temperature. An opening angle of 0.2° of the test-section's floor and ceiling was implemented in order to compensate for the thickening of the side wall BLs (constant static pressure in the empty test-section). With a flow velocity of 50 m/s and a reference cord length of 0.6 m ($\Lambda = 2,2$), a Reynolds number of 2 millions can be achieved. The position

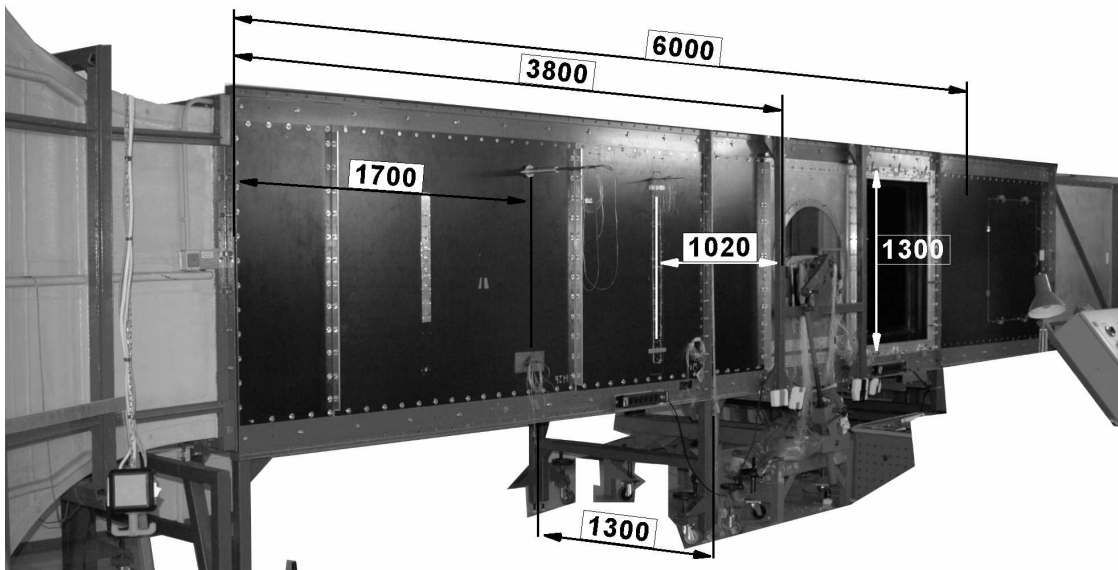


Figure 5: MUB test-section with integrated 2 element airfoil (DLR-F 15 contour)

of the model was 3.8 m downstream the nozzle (Figure 5). This far downstream position was chosen to allow subsequent investigations that require an additional device in the test-section upstream the airfoil model. The wing model's centre of rotation was located at $x/c=0.561$ and at 50 % of the wind tunnel's height (Figure 2). The static reference pressure for the calculation of c_p was averaged from the static fraction of two Prandl probes, positioned in the vertical centre plain of the wind tunnel 1.7 m downstream of the tunnel nozzle. Additionally, the static pressure distribution was measured in the tunnel's ceiling and floor at approximately 500 mm intervals.

3 Results

Every model test set-up suffers from constraints. The major limit in the described test set-up was the limited dimension of the wind tunnel and the adjunct interaction of comparatively thick side wall BL with the airfoil flow. The thickness of the BLs is closely connected to the far downstream position of the model within the wind tunnel, which was necessary for subsequent disturbed flow investigations. The measured stall behaviour of the DLR-F 15 in 2e-configuration should preferably be clear from side wall BL effects and alike for better CFD comparison. Therefore, the experiments were designed in order to identify and minimise different sensitivities of the set-up with respect to stall behaviour, 2-D flow in the centre section, and repeatability. Therefore, fixation of transition location, the local leading edge droop angle, the geometry of the local leading edge droop device and the introduction of flap-tracks as structural support were investigated and optimised as described individually in the following chapters. Finally the achieved comparability of the experiments towards wind tunnels of larger size was evaluated.

3.1 Fixation of transition location

The location of airfoil transition is depending on the Reynolds number [11] [4]. The higher the Reynolds number, the closer to the leading edge transition happens. A Reynolds number of 2 millions, achieved within the testing facility, was supposed not to be enough to create a fully

turbulent flow over the airfoil, whereas airfoils of industrial planes in free flight see very high Reynolds numbers (even during starting and landing) and accordingly tend to have a fully turbulent flow over the whole airfoil. The investigated airfoil exhibited a laminar separation bubble at the leading edge under testing conditions. As laminar separation bubbles have great influence to the flow and do not represent the modeled reality, the fixation of transition location was one of the first sensitivity investigated. It became obvious during tests with tufts, that very small imperfections in the surface of the leading edge region have strong influence on transition. Multiple attempts to trip the BL with 0,05 mm thick and 4 mm wide self adhesive tape were carried out. With the help of the lift-curve characteristics, the best results were identified when exclusively utilising the change in surface roughness caused by the span wise measurement holes, respectively pneumatic tripping holes. More precisely, the taps where plugged from the inner airfoil side, so that no pressure triggering could take place. The rest of the laminar separation bubble, that is locally destroyed by the influence of the holes' roughness, can be seen in Figure 4 b. On the other hand, the flap's BL was not tripped. However, validations with a stethoscope revealed a quasi static transition area at 0.3 flap cord-length (this is equal to $0.965 x/c$).

3.2 Local leading edge droop



Figure 6: Side wall droop-nose (SWDN) with 15° droop angle

forth referred to as the step-nose (Figure 6). The step-nose was experimentally realised by inserting a wedge into a spanwise slit located in the upper side of the main-element. A second 130 mm long slit, perpendicular to the span, margined the SWDN's span. The inserted wedge pushed the SWDN downward without the need of a hinge since CRP is a relatively flexible material. Hence the SWDN's assembly, the step-nose has no continuous geometry from the drooped to the normal leading edge. For sensitivity investigations the increase in droop was done in steps of 5° , from 0° to 20° . The pressure distribution (Figure 7) taken along the centre section (Figure 4) shows a sensitivity of the lift to the droop angle. At an angle of attack of 4° (Figure 7) the strongest influence arises on the suction side of the airfoil. The suction peak of the main-element is distinctly influenced by the droop angle in a way, that the stronger the droop is, the more the suction peak is reduced. Unfortunately this correlation is smaller than the sensitivity to the set-up's imperfections described later, and therefore was not consistent throughout all studied cases. Additionally, there is also a minor effect on the separation of the flow at the flap's trailing edge.

The reduction of side wall BLs' influence to the airfoil flow was the main topic of this experimental campaign. To solve the problem the mean selected was a locally drooped nose of the main element. The 130 mm span (10 % wingspan) of the side wall droop-noses (SWDN) has been defined based on results of side wall BL measurements. These measurements were realised using a Prandl probe positioned 1.02 m upstream of the airfoil. It was found that the side wall BL has an averaged thickness of approximately 70 mm on this position, making the 130 mm SWDN span a reasonable choice. This section presents the investigation into the sensitivity of SWDNs' droop angle with a configuration that is hence-

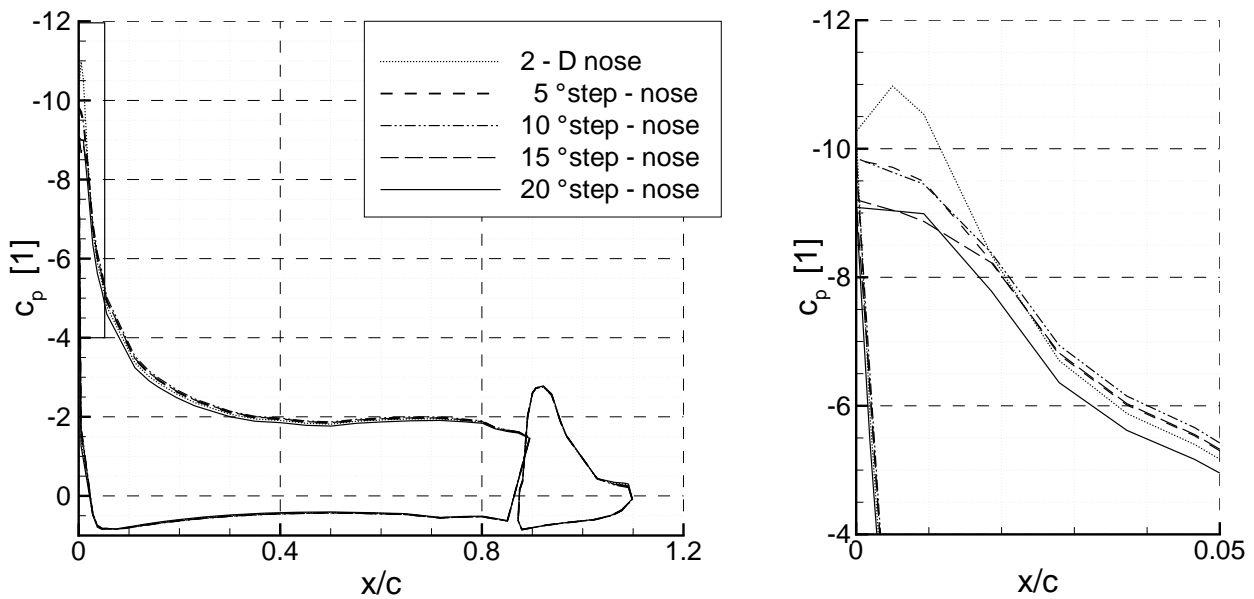


Figure 7: Pressure distribution in centre section at $\alpha = 4^\circ$

The reproducibility of the lift-curve (Figure 8) is also a phenomenon related to the droop angles. The various lines in the graphs represent different surveys with the same SWDN and wing-flap configuration. Between each survey the test set-up was changed to another droop angle. The averaged maximum lift and maximum angle of attack are respectively marked

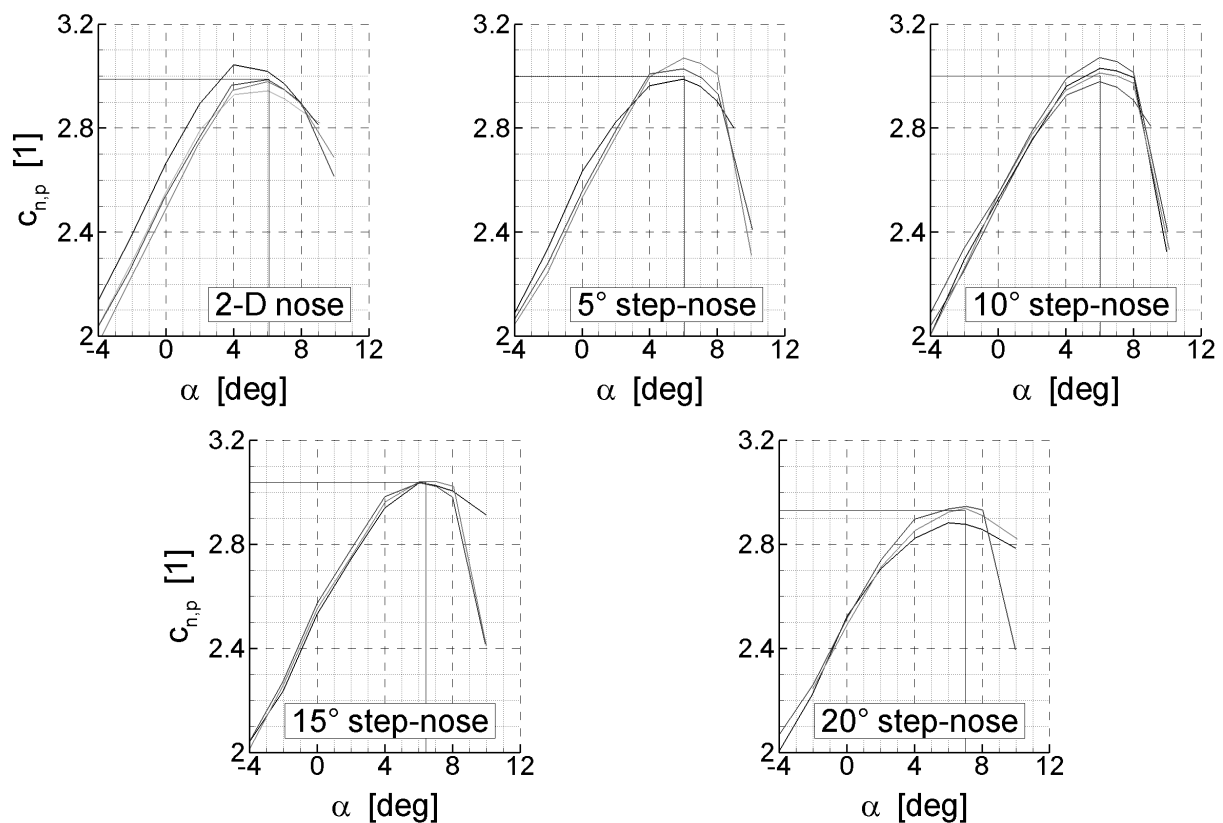


Figure 8: Comparison of lift versus angle of attack with increasing droop angle

to illustrate their shift with increasing droop angle. Hence, the increase of the droop angle improves reproducibility, whereas the maximum lift $c_{n,p}$ slightly increases. Best reproducibility and acceptable characteristics of the lift versus angle of attack curve were achieved with 15° droop angle.

The results indicate that the local decrease in angle of attack discharges the BLs and thus improves reproducibility and maximum lift up to a certain droop angle, after which the increased camber and bending of the profile contour produces a negative effect on the maximum lift and reproducibility. Discrepancies in the reproducibility results could also be explained by uncertainties in the geometry of the experimental set-up. Such uncertainties were encountered in the droop positioning where the use of wedges engendered an angular uncertainty in total, as well as in symmetry (right versus left side), of $\pm 0.5^\circ$. This amount of uncertainty was deemed high, especially for small droop angles. These findings resulted in improved SWDN design, described in the subsequent sections. It should be noted that this investigation was part of a preliminary inquiry and was carried out with a slightly different wing-flap configuration than fs#1 (ref. to “experimental set-up”). Therefore comparisons with subsequent pressure distributions and lift-curves are not fully valid. However, the configuration was very close to fs#1 and hence the investigated flow phenomena can be transferred to fs#1 configuration.

3.3 Geometrical sensitivity (local leading edges)

The reduction of the side wall BLs’ influence on airfoil stall behaviour was achieved by introducing SWDNs. To understand and optimise the effect of SWDN the geometrical sensitivity was investigated, and three different pairs of noses were considered therefor: a nose without droop, the 2-D nose (Figure 9 a), a step-nose with 15° droop angle (Figure 9 b), and a smoothed-nose, also with 15° droop angle (Figure 9 c). The 2-D nose was used as a reference case for the pure

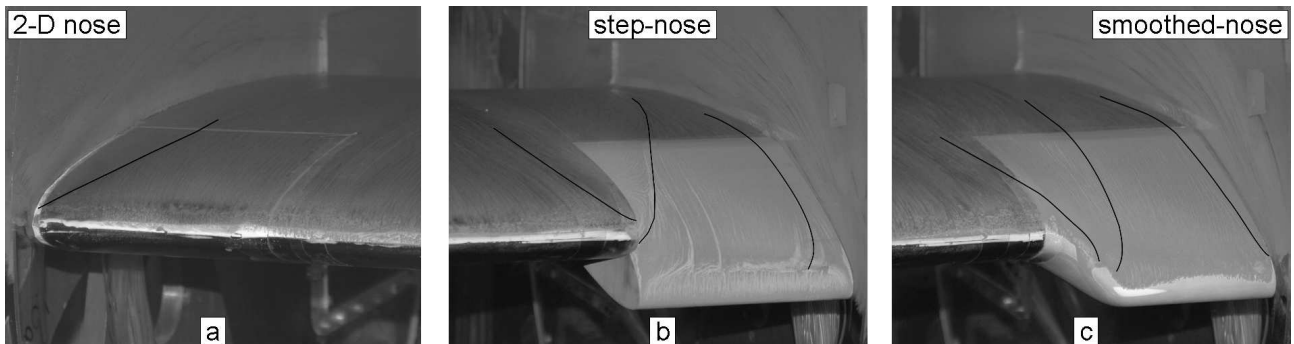


Figure 9: Side wall droop-nose versions investigated

2-D airfoil, whereas the step-nose for droop angle sensitivity investigations. The smoothed-nose was intended to facilitate CFD calculation while maintaining the benefit of the step-nose design. The smoothed nose design was also used as a reference to investigate the effects of the sharp geometrical step on the flow. The question to answer was, if the sharp step has an influence to the flow character, or if the described decrease in angle of attack and the increase of camber and contour bending are the only responsible factors for the improved flow. The investigation was performed in fs#1 configuration with more consideration to aforementioned sensitivities. This was accomplished by the screw installation of the different noses (as opposed to wedge inserts).

Oil flow visualisation pictures are footprints of the flow and as such deliver an impression of the flow phenomena. The edge effect of the different noses is shown in the oil flow visualisation

pictures Figure 9 . The lines in Figure 9 were used to highlight the approximate regions of disturbances. As shown in Figure 9, the introduction of a droop-angle (step- or smoothed-nose) generate two additional Δ -shaped disturbances at the droop angle leap, which result from the engendered local vortices.

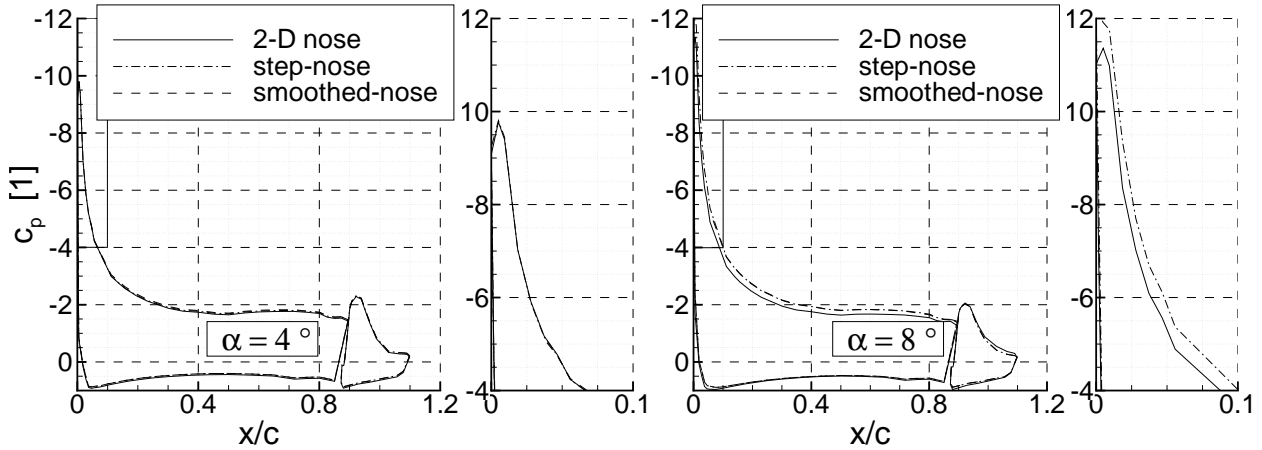


Figure 10: Sensitivity of the pressure distribution to droop-noses geometry

To evaluate the influence of the interactions of the BLs on the airfoil stall behaviour, static pressure measurement on the airfoil's surface is a reliable and fast solution. Based on the preliminary inquiry towards the geometrical sensitivity, it was expected that for the drooped noses, compared to the 2-D nose the effect of reduced suction peak would appear in static pressure measurements (compare with Figure 7). These expectations were fulfilled, but shifted to smaller angles of attack for the refined set-up. At $\alpha = 4^\circ$, the pressure distributions of the 2-D and the drooped nose configurations are very similar (Figure 10). At higher angles of attack ($\alpha = 8^\circ$), the drooped configurations develop a smaller c_p throughout the airfoil's upper side (Figure 10).

On the other hand, the step-nose and the smoothed-nose configuration have a similar pressure distribution. From these observations it can be concluded that the sharp edge of the step-nose does not additionally contribute to the effect of local droop. Comparing the 2-D nose configuration to the drooped configurations, the higher suction peak for small angles of attack (smaller than $\alpha = 4^\circ$) and the lower under pressure on the main-element for higher angles of attack, cause a lift that is inversely proportional to the angles of attack, as can be seen in Figure 11. A straighter lift-curve for the drooped nose configuration can be seen in Figure 11, what indicates a lower sensitivity to flow disturbances. To ascertain this observation, it is helpful to analyse further oil flow visualisation results (Figure 12). Similar to the analyses at the beginning of this section, the boundary of the side wall disturbances are marked with solid lines. Neglecting the flap-track influence and the separation of the flap-flow

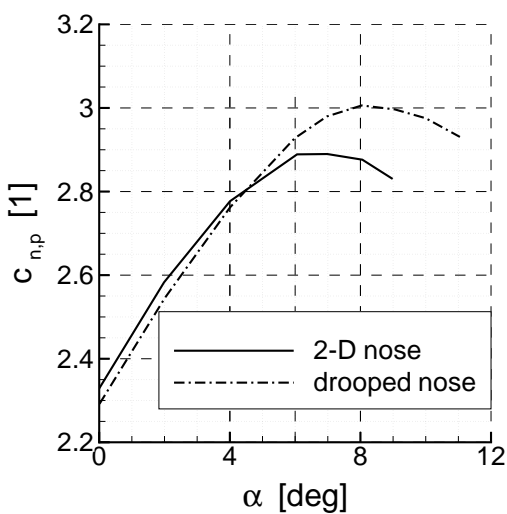


Figure 11: Lift versus angle of attack for 2-D and drooped noses

the effect of the side wall BLs on the airfoil flow is observed to be much stronger with the 2-D noses than with drooped configurations (Figure 12). This phenomenon may be due to the longitudinal vortex emanating from the drooped nose, which generates a vertical motion towards the wall and keeps the side wall disturbances slim. The higher lift, observed with the

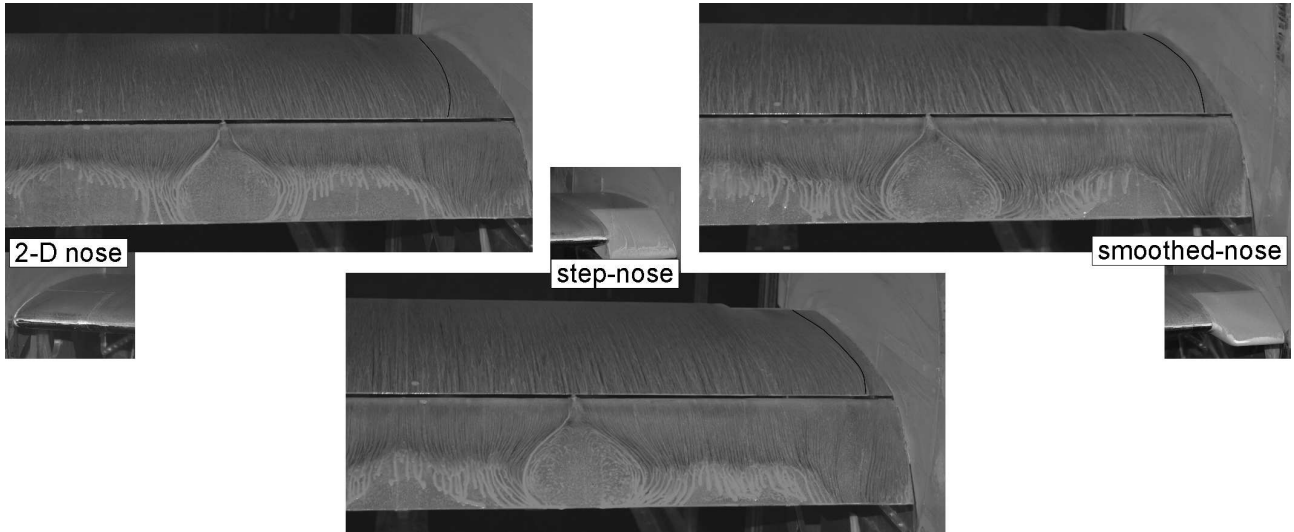


Figure 12: Oil flow visualisation of BL interactions at $\alpha = 4^\circ$

2-D profile for small angles of attack can be explained with two mechanisms. On the 2-D nose side: The blockage of the “free” airfoil flow in the centre section, due to the large side wall disturbances with the 2-D nose, results in a higher velocity and therefore in a lower pressure minimum. On the drooped nose side: The down-force caused by the lift distribution, which has a strong gradient at the drooped nose region. The uneven distribution of lift causes “free edge vortices” along the outer sections that induce lower effective angles of attack to the centre section. On the other hand, higher angles of attack force a shift in the maximum lift towards smaller $c_{n,p}$ regarding the 2-D nose configuration. This contradiction may be explained by the blockage of the “free” airfoil flow as well. Whereas drooped configurations exhibit slim side wall BL effects, the 2-D nose configuration shows a propagation of the side wall BL effects over the entire wingspan (Figure 13). The flow over the main-element, for the 2-D nose configuration, seems to detach at smaller angles of attack.

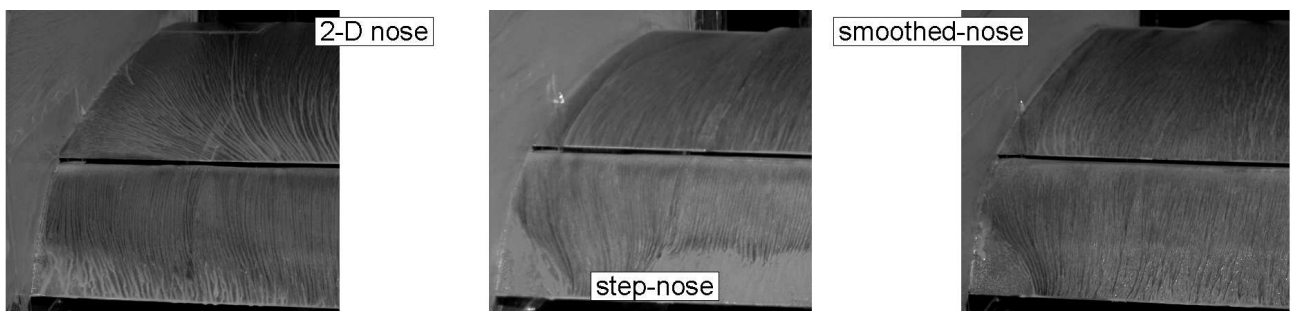


Figure 13: Oil flow visualisation of BL interactions at $\alpha = 8^\circ$

3.4 Sensitivity towards flap-tracks

As the flap is an airfoil with a high aspect ratio ($\Lambda = 7.7$) and exposed to diverse flow separations, it is sensible to structural vibrations. Therefore, the flap was rated very stiff and build out of CRP. To further improve its resistance towards vibrations the flap's natural frequency was augmented by structural pre-load. Contrary the idea of free flow, the mean of additional structural supports, flap-tracks, become necessary to investigate small angles of attack where the flow detaches from the flap's surface. That is the reason for the configuration to be investigated twice. Once only for large angles of attack and without flap-tracks and once with flap-tracks to define their influence. The influence of flap-tracks on the flow characteristics is

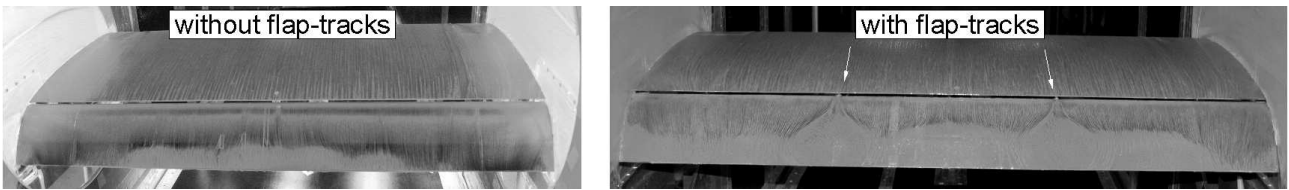


Figure 14: Oil flow visualisation of flap-track influence with 2-D nose configuration at $\alpha = 4^\circ$

observed in the oil flow visualisation pictures of Figure 14 and Figure 15. As the figures show, additional focal points occur in the trails of the devices compared to the configuration without flap-tracks. Furthermore, the BL separation over the flap starts closer to the flap's leading edge. The wavy characteristic of the flow separation over the flap remains, but becomes somewhat more 2 dimensional and more continuous over the wingspan. Moreover, the influence of the focal points towards the centre section of the flap is small, as the separation characteristics remain comparable. This observation is not only restricted to the 2-D nose configuration (Figure 14), but extends to the step-nose configuration (Figure 15) as well. The evaluation of



Figure 15: Oil flow visualisation of flap-track influence with step-nose configuration at $\alpha = 4^\circ$

pressure distribution at 4° angle of attack (Figure 16) also demonstrates the influence of the flap-tracks on the airfoil-flow along the centre section. As seen in the figure, the addition of flap-tracks decreases the suction peak of the main element and by association increases the suction's side pressure. That is due to the increase of the flap's suction peak. Analysis of the lift-curves reveals a tendency of stall behaviour towards smaller angles of attack for the configuration without flap-tracks (Figure 17). One reason for the lift-curve's shift is the "undefined" gap between wing and flap without flap-tracks. However, the configuration is highly sensitive to the gap and oppose the trailing edge of the main element, which does not bend span wise under flow charge, the flap does. It should be noted here that measurements at an angle of attack smaller than 4° were not possible without flap-tracks, because of the flap's vibration along its natural frequency. See introduction of this section on this.

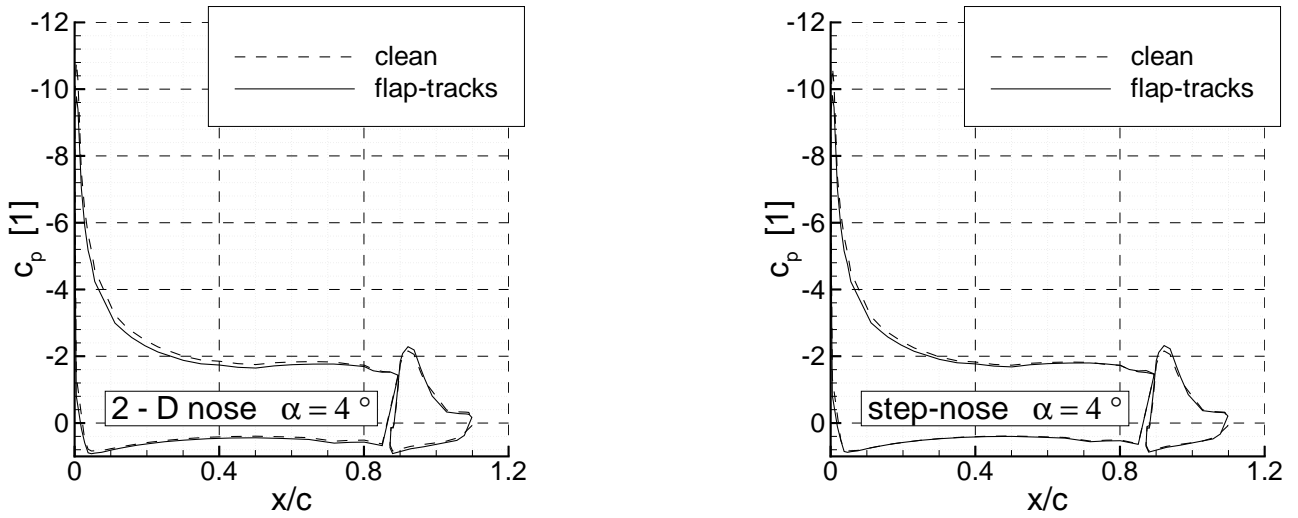


Figure 16: Pressure distribution at $\alpha = 4^\circ$ with and without flap-tracks

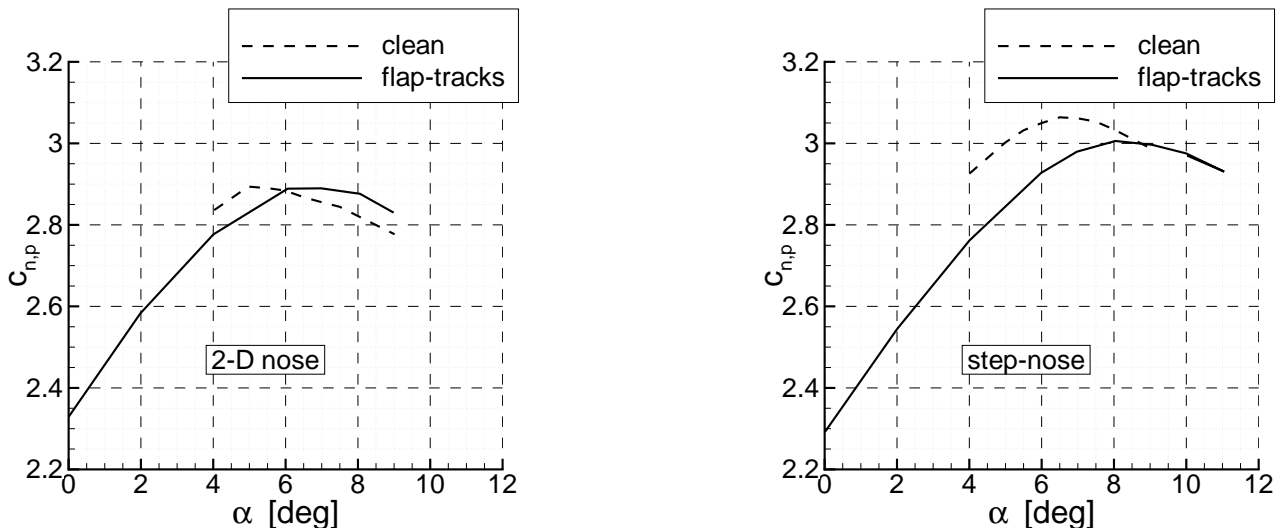


Figure 17: Lift versus angle of attack with and without flap-tracks

3.5 Comparison with commercial wind tunnel results

In order to evaluate the advantages and disadvantages of SWDNs and flap-tracks and putting results together, a comparison with results acquired in industrial wind tunnels is necessary. The

wind tunnel	cross-section m^2	aspect ratio Λ
MUB	1.3×1.3	2.2
DNW-KKK	2.4×2.4	4
DNW-NWB	3.25×2.8	4.7

Table 1: Comparison of wind tunnel dimensions

following comparison covers closed-loop return wind tunnels with closed test-sections without slots at ambient temperature and under atmospheric measurement conditions using DLR-F 15

shaped 2 element airfoil models with a cord length of 0.6 m (Table 1). Whereas the DNW-KKK is a medium sized wind tunnel with cryogenic capability, the displayed results were generated under atmospheric measurement conditions. Figure 18 shows two NWB lift-curves, to illustrate the influence of little changes in the experimental set-up for a medium sized wind tunnel. For the case of NWB, a variation of the flap material (aluminum versus CRP) and fixation of transition location, led to the displayed differences. The results show a similar lift-curves match for all wind tunnels. The lift-curve, for the step-nose configuration in the current study is almost equal to that of the KKK's, whereas DNW's results are lower in lift and shifted to slightly higher angles of attack. Note that all lift versus angle of attack curves shown in Figure 18 are

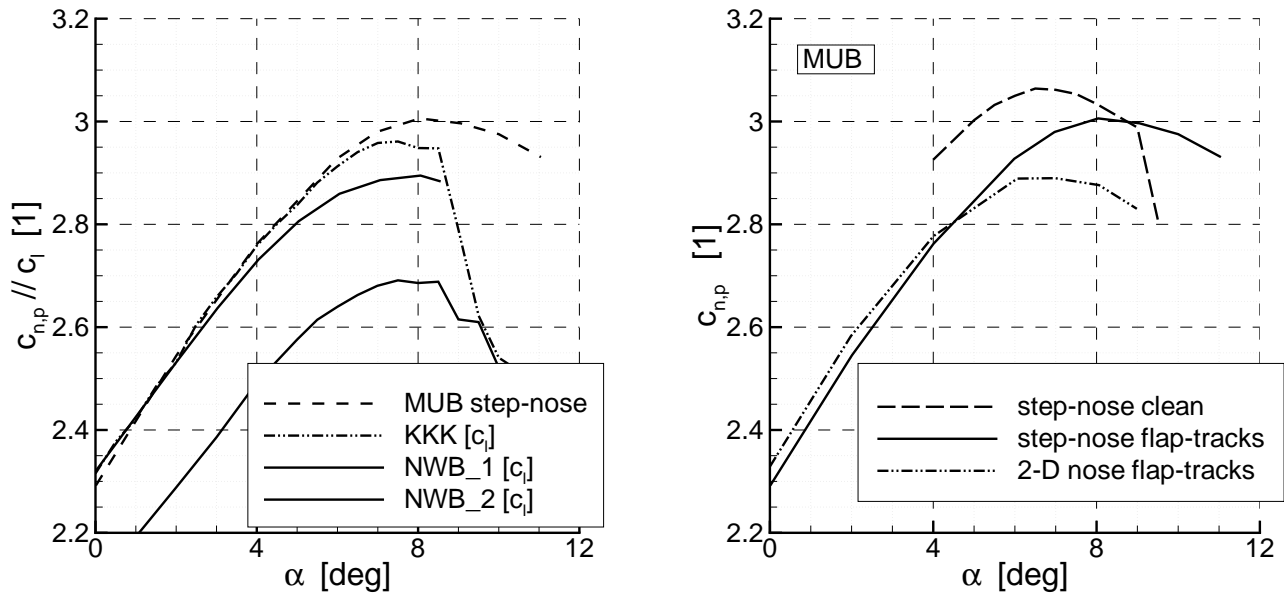


Figure 18: Comparison of lift versus angle of attack curves; in different wind tunnels a of different experimental set-ups b

for uncorrected measurement results. This means they are displayed without any corrections concerning the influence of the wind tunnel geometry. In addition the lift of the airfoil measured in the MUB is displayed as $c_{n,p}$ (see “experimental set-up”), whereas that of KKK and NWB is quantified using c_l , which factors in the drag. The displayed data of DNW-NWB and DNW-KKK was acquired during flow control analysis [14] in the context with LUVU IV m-fly.

The influence of the flap-tracks and the SWDN have been discussed before and are displayed incidentally again, to give an idea of their influence relative to that of the tunnel. Although an airfoil with a cord length of 0.6 m is generally too big for a test cross-section of $1.3 \times 1.3 \text{ m}^2$ at high angles of attack, results show that a good agreement with commercial wind tunnel characteristics, where the side wall BL effects are way smaller, can be achieved if care is taken to treat the interferences.

4 Conclusion

This publication describes investigated sensitivities and actions that have been taken to enable reasonable measurements on a two-element high-lift airfoil (DLR-F 15 in fs#1 configuration) in a small sized wind tunnel with emphasis on the determination of the stall behaviour. The measurements were made in a small sized wind tunnel, as a very comprehensive validation

database for CFD computation was required at a reasonable effort. The first step of the investigation was the valuation of the airfoil's sensitivity towards the location of transition on the main element. The fixation of the transition location to a reasonable region was executed by augmentation of the leading edge's roughness with holes. As a second step the side wall BLs' influence on the airfoil BL was compensated by the use of local leading edge droop. A sensitivity study resulted in 15° droop angle to be very effective in sense of reproducibility, as well as in sense of pressure distribution. The third step was the investigation of the sensitivity of the system towards geometrical adaptations of the SWDNs. It was proofed, that a SWDN optimised towards CFD brings along the same benefits as the step-nose does. Accordingly, the step-nose's sharp geometrical step has no additional influence on the flow. Between step two and three the flap-tracks were applied to the airfoil configuration and the investigation of this influence is described as step four in this publication. The flap-tracks showed a very good performance in terms of structural support and an acceptable influence to the global airfoil flow. As expected, local disturbances in the trail of the tracks were created, but the over-all flow separation behaviour of the flap did not severely change. However from the point of stability and reproducibility, flap-tracks are indispensable. As last step the integrity of the measures taken had to be proved. Therefore, the achieved results were compared to those of other wind tunnels. The achieved quality in measurements with an airfoil of small aspect ratio in a small wind tunnel are promising and in good comparison to commercial wind tunnel results. The test set-up has been optimised regarding reproducibility and simple operation, in order to generate repayable results. It has been realised to enable a quasi 2-D flow along the centre section, so comparability to 2-D CFD computations is given. The generation of a validation data base has started on this basis. However, blockage and down force effects seem to lead to a "good-natured" lift-curve for airfoils with drooped noses, the phenomena still need to be investigated more closely. PIV measurements and 3-D CFD computations are planned.

Acknowledgments

The members of the FOR 1066 research group gratefully acknowledge the support of the "Deutsche Forschungsgemeinschaft DFG" (German Research Foundation) which funded this research. Further acknowledgment for their support deserves the research group of LUVO IV m-fly, namely J. Wild, V. Ciobaca, and M. Sitzmann from the DLR, and M. Casper (ISM).

References

- [1] Arnott, A., Schneider, G., Neitzke, K.-P., Agocs, J., Schröder, A., Sammler, B., Kompenhans, Jürgen. "Detailed Characterisation, using PIV, of flow around an Airfoil in High-Lift Configuration." In: Particle Image Velocimetry: Recent Improvements Proceedings of the EUROPIV 2 workshop held in Zaragoza, Spain, 2003
- [2] Ashok, G., Broughton, B. A., McGranahan, B.D., Selig, M. S.: "Design of low Reynolds Number Airfoils with Trips", Journal of Aircraft, Vol. 40 no. 4, 2003
- [3] Birkemeyer, J.: "Adapted Wind Tunnel Walls for a Swept Wing Experiment", New Results in Numerical and Experimental Fluid Mechanics II , AG STAB
- [4] Gault, D.E.: "A correlation of low-speed airfoil stalling characteristics with Reynolds number and airfoil geometry", NACA-TN-3963

- [5] Gleyzes, C., Capbern, P.: “Experimental Study of two Airbus/Onera airfoils near stall conditions. Part I: Boundary Layers”. *Aerospace Science and Technology* 7, pp 439-449, 2003.
- [6] Gursul, I., Deng, Q.: “Effect of Leading-Edge Flaps on Vortices and Vortex Breakdown”, *Journal of Aircraft*, Vol. 33 no. 6, 1996
- [7] Godard, G., Foucaut, J.M., Stanislas, M.: “Control of decelerating boundary layer. Part 1 /2: Optimization of slotted jets vortex generators.”, *Aerospace Science and Technology*, Vol 10, 07-2006, 394-400
- [8] Keirsbulck, L., Labraga, L., Haddad, M.: “Influence of blowing on the anisotropy of the Reynolds stress tensor in a turbulent channel flow”, *experiments in Fluids*, 40-2006, 654-662
- [9] Lachmann, G. V.: “Boundary Layer and Flow Control Its Principles and Application”, Pergamon Press Vol. 1 / 2, 1961
- [10] Meyer, O., Nitsche, W.: “Update on progress in adaptive wind tunnel wall technology”, *Progress in Aerospace Science*, Vol 40, 04-2004, 119-141
- [11] Pope, A., Rae, W. H., Barlow, J. B.: “low-speed wind tunnel testing”, 3 rd Edition Wiley-Interscience Publication 1999
- [12] Rasuo, B.: “On boundary Layer Control in Two-Dimensional Transonic Wind Tunnels”, *Int. conference on Boundary and Interior Layers*, Bail-2006
- [13] Scholz, P., Casper, M., Ortmanns, J., Kähler, C. J., Radespiel, R.: “Leading Edge Separation Control by Means of Pulsed Vortex Generator jets”, *AIAA 2008-837*, 2008
- [14] Scholz, P., Kähler, C.J., Radespiel, R., Wild, J., Wichmann, G.: “Active Control of Leading-Edge Separation within the German Flow Control Network”, *AIAA-2009-529*, 2009
- [15] Takeda, K., Ashcroft, G.B., Zhang, X., Nelson, P.A. :”Unsteady aerodynamics of slat cove flow in a high-lift device configuration”, *AIAA-2001-0706*, 2001
- [16] Wild, J., Wichmann, G., Haucke, F., Peltzer, I., Scholz, P.: ”Large scale separation flow control experiments within the German Flow Control Network”, *AIAA-2009-530*, 2009
- [17] Wockoeck, R., Krimmelbein, N., Radespiel, R., Ciobaca, V., Krumbein, A. :”RANS Simulation and Experiments on the Stall Behavior of an Airfoil with Laminar Separation Bubbles”, *AIAA-2006-0244*, 2006